Urban Rail Transit (2022) 8:286–295
https://doi.org/10.1007/s40864-022-00178-7

http://www.urt.cn/

ORIGINAL RESEARCH PAPERS

Research on the Bearing Performance of Prefabricated New Type Subway Track Slab with Basalt Fiber

Dan Liu[1] · Zexu Zhao[2] · Mengdi Wu[3] · Peigang Li[2,4] · Junqi Li[2] · Xiaoyi Qian[5]

Received: 10 June 2022 / Revised: 18 September 2022 / Accepted: 27 September 2022 / Published online: 4 November 2022

Abstract Currently, most ballastless tracks in Chinese subways are traditional cast-in-situ concrete structures, which require long construction progress. In contrast, prefabricated ballastless tracks can greatly reduce the construction period. However, there are few theoretical and experimental analyses on the prefabricated new type of subway slab track. Hence, to study the mechanical properties of the new type of subway track slab, static bending crack tests of one standard slab track and nine prefabricated full-scale track slabs with basalt fiber were carried out in this paper. The influence of the reinforcement arrangement method and the basalt fiber content on the performance of the track slabs was studied. Results showed that with the increase in the basalt fiber content in the range of 0.1–0.3%, the load–strain curve growth rate increased, the stiffness decreased, and the flexural resistance reduced. All the specimens exhibited a linear portion (elastic) and then a nonlinear portion (plastic) followed by flexural failure. During the elastic stage, the basalt fiber helped to improve the rigidity of the track slab. During the plastic stage, the influence of the basalt fiber content on the failure load varied with different reinforcement arrangements. With the reinforcement arrangement F2 and 0.1% basalt fiber content, the specimen had the smallest load–strain curve growth rate and the best overall flexural performance and crack resistance, and its strain was 23.35 με at an elastic limit of 95 kN. The results can provide a reference for the design of the prefabricated slab ballastless track.

Keywords New type subway track slab · Basalt fiber · Static load bending test · Reinforcing bars · Cracks · Deflection

✉ Peigang Li
lipeigang@sit.edu.cn

Dan Liu
liudan88r@chd.edu.cn

Zexu Zhao
278275951@qq.com

Mengdi Wu
815473709@qq.com

Junqi Li
932589845@qq.com

Xiaoyi Qian
540628846@qq.com

[1] Highway School, Chang'an University, Xi'an 710064, Shaanxi, China

[2] School of Railway Transportation, Shanghai Institute of Technology, Shanghai 200000, China

[3] Maintenance Division of Shanghai Metro Maintenance and Support Co, Shanghai 200000, China

[4] Dalian University of Technology, Dalian 116024, China

[5] China Railway Shanghai Bureau Group Co. Ltd, Shanghai 200071, China

Communicated by Liang Gao.

1 Introduction

At present, most ballastless tracks in Chinese subways are traditional cast-in-situ concrete structures, which are cost-effective and have good overall performance. However, they have some obvious disadvantages, such as long construction process, high labor intensity, poor quality controllability, and poor working environment. During operation, cast-in-situ ballastless tracks tend to crack more easily than prefabricated ballastless tracks, which can then lead to steel corrosion and loss of bearing capacity [1–4].

In addition, the maintenance of these issues is very difficult and their quality is difficult to guarantee [5]. Meanwhile, due to the continuous increase in subway train operating speed, traffic density, and the large-scale subway construction in major cities [6], the traditional cast-in-situ ballastless track can no longer meet current construction needs. With the rapid development and application of slab tracks for high-speed railways, more and more high-speed railway design and construction technologies have been applied to the subway [7, 8]. The new prefabricated subway slab track absorbs the technology of the CRTS III slab track of high-speed railway [9], which has the advantages of strong integrity, high quality and precision, good earthquake resistance, convenient construction and maintenance, etc. [10, 11]. But, unlike the CRTS III slab track of high-speed railway [12–14], the new prefabricated slab track does not contain the prestressed reinforcement, so its crack resistance is different from that of the high-speed railway slab.

Some scholars have carried out related studies of new slab tracks for the subway. Gharighoran [15] analyzed the dynamical characteristics of the subway slab track under different loads and operating conditions of the Iranian subways. Combined with the practical experience of high-speed railway slab track, Liu et al. [16] conducted the field test of a new type of subway slab track and verified the dynamic test results. He et al. [17] studied the dynamic behavior and the vibration absorption characteristics of the new slab track through field tests and numerical simulation. Liu and Xu [18] established a three-dimensional nonlinear mechanical model of a precast slab subway track to study the spatial mechanical characteristics under single and combined loads. However, there are still few theoretical and experimental analyses on the new type of subway slab track. In particular, there is still a lack of the influence of different materials on the bearing characteristics of the track structure.

Based on the existing standard new type of subway slab track, the static bending crack test of one standard slab track and nine prefabricated full-scale track slabs were carried out, and the mechanical properties of the subway slab track with different basalt fiber content and different reinforcement arrangements were analyzed. The results can provide a reference for the design of the prefabricated slab ballastless track.

2 Test Plan

2.1 Test Specimens

The test slab track is the P4700 full-size new subway slab track produced by China Railway 23rd Engineering Bureau Group Co., Ltd. The track slab is a prefabricated unit structure without prestressed reinforcement; its global dimensions are 4700 × 2300 × 200 mm. Each unit has 16 built-in 420 × 290 mm sleeper blocks. The concrete of the specimen has average compressive strength of 50 MPa at the age of 28 days. The reinforcement arrangements of the standard track slab (X0) are shown in Fig. 1 and Table 1.

In this paper, there are three reinforcement arrangement methods (F1, F2, F3):

F1: compared with the standard new subway track slab, the N9, and N10 reinforcements were removed;
F2: compared with the standard new subway track slab, the diameter of the N1 and N2 steel bars was reduced from 14 mm to 12 mm, while the N9 and N10 steel bars were removed, and the rest of the reinforcements were kept;
F3: the N1, N2, N3, N4, and N5 were replaced by smaller steel bars with Φ10 mm in diameter, while the N9 and N10 reinforcements were removed, and the rest of the reinforcement were kept.

With each reinforcement arrangement method, three track slabs were prefabricated with 0.1%, 0.2%, and 0.3% basalt fiber, respectively. Meanwhile, one standard subway slab track X0 was prefabricated. Therefore, a total of 10 track slabs (as shown in Table 2) were tested to study the mechanical properties of new prefabricated subway slab tracks with different basalt fiber content and different reinforcement ratios.

2.2 Testing Method

A three-point load static test was used to study the general flexural behavior of the new type of track slab with basalt fiber. The static test loading setup is illustrated in Fig. 2. At each short edge, a pair of steel pillars and a 3000 mm × 200 mm beam were installed at 550 mm from the edge to simulate the support condition. A spreader beam 2000 mm in length was placed longitudinally at the top of the middle plate. The load was applied on the spreader beam with 50 tons oil jack so that the pressure could be applied uniformly to the middle of the track slab.

The static loading test was divided into two stages, the pre-loading stage (the first cyclic loading) and the formal loading stage (the second cyclic loading). Pre-loading can help to stabilize the relationship between the load and the track slab deformation, allowing the structure to work under normal conditions and reducing test error. Both pre-loading and formal loading were conducted with stepwise loading at a loading speed of 0.5 kN/s. All faces of the track slab were visually inspected to check and mark these limits before the test. In the first cyclic loading stage, the load was 10 kN, which was divided into five stages in

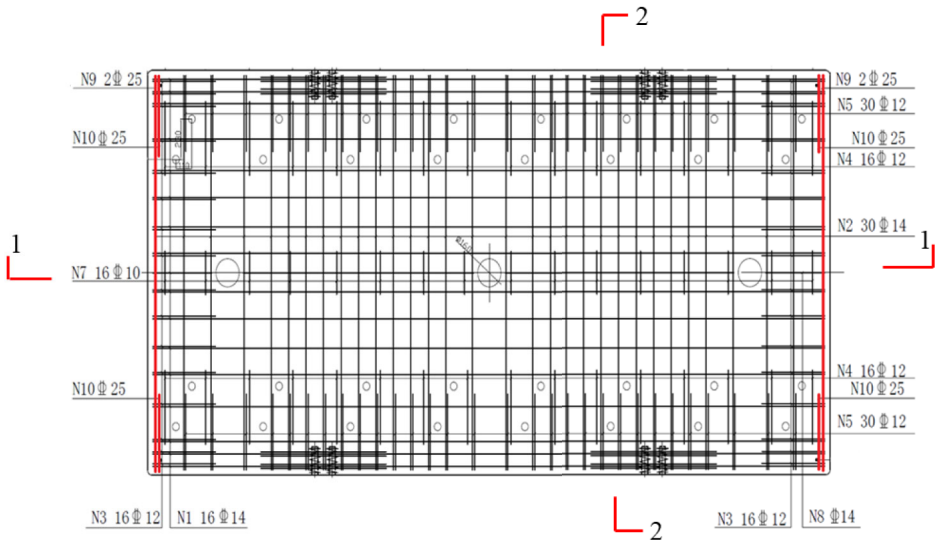

a general layout plan of reinforcement

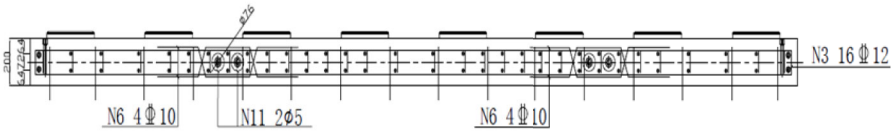

b 1-1 cross-section

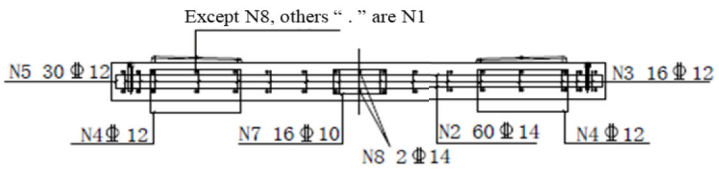

c 2-2 cross-section

Fig. 1 The reinforcement arrangement of the standard new type subway track slab X0

Table 1 Properties of rebar

Rebar	Diameter (mm)	Number	Length (m)	Yield strength (MPa)	Rebar	Diameter (mm)	Number	Length (m)	Yield strength (MPa)
N1	14	32	4.703	150.496	N7	10	16	0.85	13.6
N2	14	60	2.317	139.02	N8	14	2	0.9915	1.983
N3	12	32	0.96	30.72	N9	25	4	4.626	18.504
N4	12	32	1.538	49.216	N10	25	4	0.932	3.728
N5	12	60	0.932	55.92	N11	5	8	1.36	10.88
N6	10	16	1.034	16.544					

increments of 2 kN per stage. After each stage, it was held steady for 3 min to observe the apparent changes in the track slab. The second cycle was loaded in the same way as the pre-loading stage, but with 5 kN per stage. During the test, the occurrence and propagation of cracks in the track slab were focused until the rebar yield.

Figure 3 shows the layout of measurement locations of strain gauges and linear variable differential transformers (LVDTs). On the top surface (A), there are eight strain gauges used to measure the longitudinal strain of the track slab. On the bottom surface (B), measurements were located at the 1/4, 1/2, and 3/4 cross-sections, each section has three longitudinal strain gauges and three LVDTs. On the side surface (C and D), there were three strain gauges located at the 1/4 and 3/4 cross-sections. Five strain gauges were located at the 1/2 cross-section of surface C, and three

Table 2 Definition of each specimen

Specimen	Reinforcement arrangement	Basalt fiber (%)	Specimen	Reinforcement arrangement	Basalt fiber (%)
X1	F1	0.1	X6	F2	0.3
X2	F1	0.2	X7	F3	0.1
X3	F1	0.3	X8	F3	0.2
X4	F2	0.1	X9	F3	0.3
X5	F2	0.2			

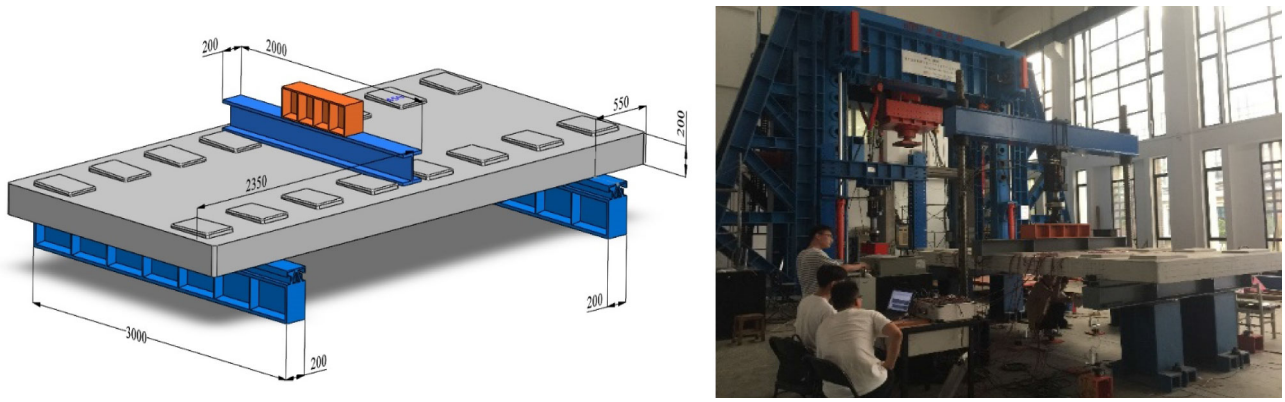

a diagram of the test setup

b site scene of the test setup

Fig. 2 Static load test setup

strain gauges were located at the 1/2 cross-section of surface D (as shown in Fig. 4).

3 Results

3.1 Strain of Track Slab

Figure 5 depicts the load–strain curve of the standard slab X0. From Fig. 5 it can be seen that when the load is less than 110 kN, almost all the stress–strain relations are linear, and the overall structure of the track slab was in the elastic stage. When the load exceeded 110 kN, the strain of each measuring point increased nonlinearly with the increase in load, and the structure entered the plastic deformation stage (yield stage). At the elastic limit, the maximum tensile and compressive strains of the track plate were 120.39 με and 354.11 με, respectively. In the elastic stage of the test piece X0, the measured strain at points 5, 6, 7, and 8 on surface A was larger than the strain at the points of the axisymmetric distribution. This was mainly because the support beam moved slightly during the test, resulting in a difference in the compressive load on both sides. A sudden change in strain was observed at measured points 1, 2, and 4 when the load reached 110 kN, 110 kN, and 80 kN, respectively. Combined with the observation of the field test, new cracks occurred at different degrees on the bottom surface corresponding to the measuring points. Strain gauges on side surfaces (C and D) and close to surface A, were under compressive conditions, and the amplitude of the strain was low. Compared with surfaces A and surface B, the strain points on surfaces C and D entered the plastic stage with a certain lag. Due to the overall tension of surface B, the slab bottom cracked when it was loaded to a certain level, and some strain gauges on the bottom failed. The overall strain rate of the standard specimen X0 in the elastic stage was smaller than that in the plastic stage, and it was more significant for the strain at the measured points on both sides of the distribution beam. At the late loading stage, due to the influence of the redistribution of the force and the crack, some of the measured values of the strain gauge changed between tension and pressure and even failed.

To analyze the influence of basalt content and reinforcement arrangement methods on the crack resistance of subway slab tracks under static load, this paper focused on analysis of the strain gauges on the tensile surface B.

Figure 6 shows the load–strain curves of track slabs with different volume content of basalt fiber under the same reinforcement method. With the reinforcement arrangement F1, the strain of specimens X1, X2, and X3 increased slowly with the increase in loading, and the structures were

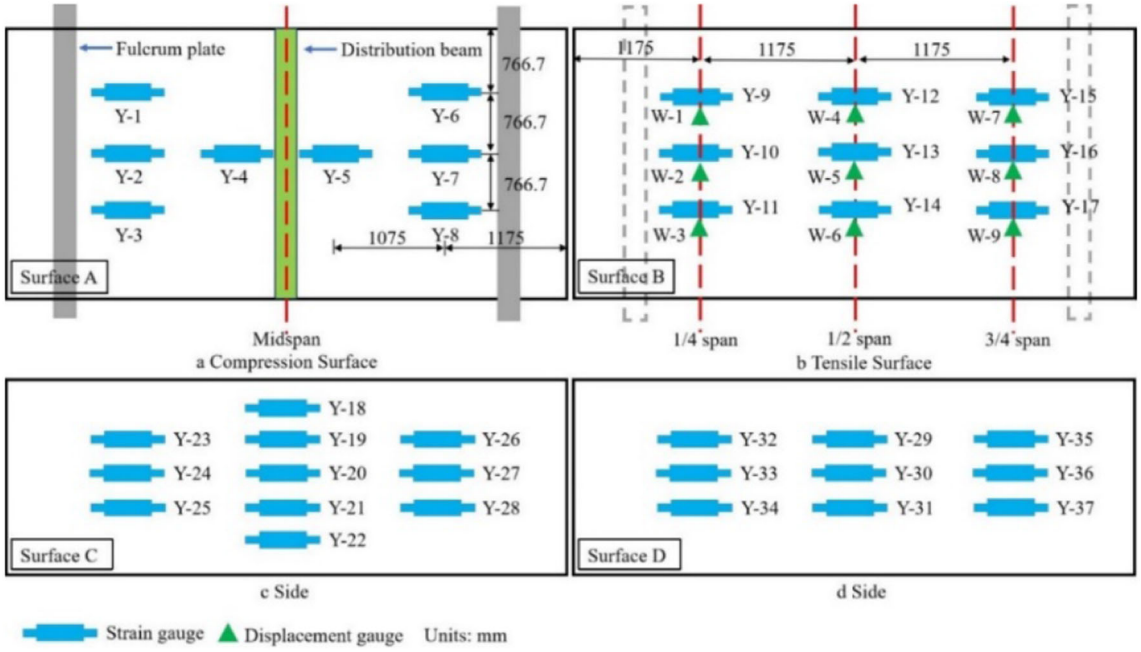

Fig. 3 Layout of measurement locations

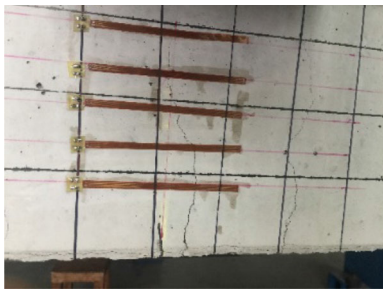

Fig. 4 Site layout of mid-span strain gauge at plane C of track slab

in the elastic stage before 45 kN, 75 kN, and 60 kN, respectively. Among them, the strain of specimen X1 was the smallest, and the maximum strain corresponding to the elastic extreme value was 29.15 με, while the strain of specimen X3 with 0.3% basalt fiber content was the largest, reaching 52.48 με. As each specimen entered the yield stage, the load–strain curve exhibited a nonlinear change, and the cracks in the track slabs increased obviously. After the three specimens were loaded to 110 kN, 110 kN, and 115 kN, respectively, the structure entered the failure

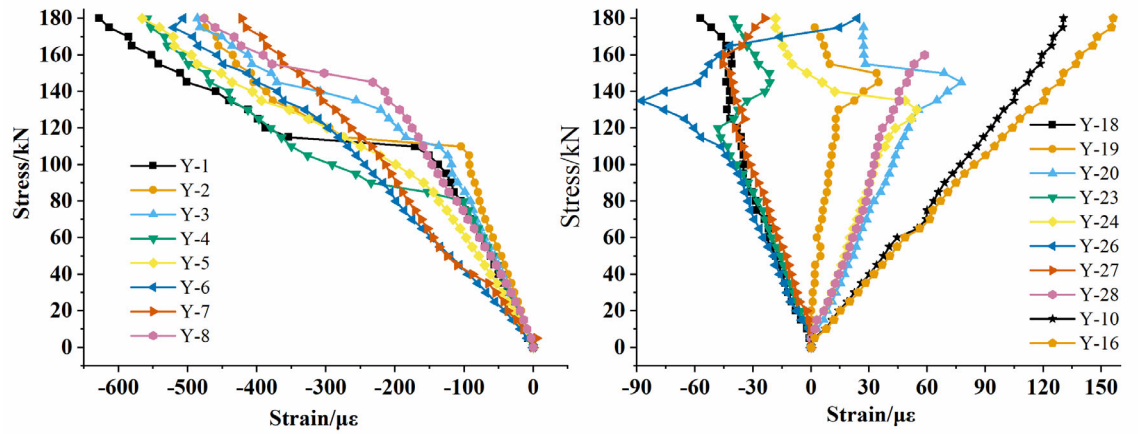

a Load-strain curve of compression surface

b Load-strain curves of side and tension surface

Fig. 5 Standard track slab X0 load–strain curve

stage, and part of specimen X3 went from tension to compression state.

With the reinforcement arrangement F2, specimens X4, X5, and X6 entered the yield stage at 95 kN, 55 kN, and 65 kN, respectively. The load–strain curves showed nonlinear characteristics, and the corresponding maximum strains were 23.35 με, 47.19 με, and 67.22 με, respectively. The bending strength of specimen X4 with 0.1% basalt volume content was obviously larger than that of specimens X5 and X6, and the mutation amount of specimen X4 at the structural failure node was smaller than the elastic limit strain of X1. Meanwhile, as the content of basalt fiber increased, the flexural behavior of specimens X5 and X6 decreased slightly, which was consistent with the conclusion in reference [19] that when the strength level of concrete is C50, the structural performance of concrete will decrease with an increase in the volume content of basalt.

With the reinforcement arrangement F3, due to the reduction of the reinforcement diameter, the structural yield strength dropped sharply. At a load of 20 kN, there was a sudden change in the strain of the track slab, and the load was unloaded and the strain fell back. After that, as the load increased, the structure entered the stage of plastic deformation, and the strain continued to rise in a nonlinear state. During the loading cycle, the strain growth rate and strain of the specimen were larger than those of F1 and F2. It can be seen that much reduction in the diameter of the reinforcement may reduce the structural performance of the track slab.

Figure 7 shows the load–strain curves of track slab specimens with different reinforcement methods for the same basalt content. When the admixture content was 0.1%, the flexural performance of specimen X4 was obviously better than that of X1 and X7. Before the load reached 95 kN, specimen X4 was in the elastic stage, its strain growth rate was small and the strain was stable. After breaking through the elastic limit, the mutation of X4 in the plastic stage was smaller than that of the other two specimens.

When the content of basalt was 0.2%, with the decline of the structural performance of the reinforcement skeleton, the bending performance of the track slab specimens decreased, and the growth rate of strain curves was larger than that of the specimens with a 0.1% basalt volume content.

When the basalt content was 0.3%, the strain and strain growth rate of the track slab structure were larger than those of the other two groups of specimens, and the period of entering the yield stage and the structural failure stage were significantly shortened. Therefore, it can be seen that with an appropriate reinforcement, adding 0.1% basalt fiber can improve the structural performance of track slabs. At the same time, too much basalt volume will reduce the flexural mechanical properties of the track plate.

It can be concluded that the elastic limit and strain of the X4 track slab were superior to those of other specimens with different reinforcement arrangement methods and basalt fiber content. According to the railway concrete structure design code and the new subway slab track quality acceptance technical standard, the reference load of the static load anti-crack test of the track plate is not less than 25 kN, and specimens X0–X6 all meet the test requirements, while the X7–X9 specimens begin to show concrete cracking, strain mutation and deflection increase near 20 kN. Therefore, reinforcement F2 and the addition of 0.1% basalt fiber are beneficial for improving the mechanical properties of the track slab, while reinforcement F3 has a negative effect on its performance.

3.2 Deflection of Track Slab

As shown in Fig. 8, all the specimens exhibited a linear portion (elastic) and then a nonlinear portion (plastic) followed by flexural failure. However, with different reinforcement arrangements and basalt fiber content, the specimens showed different deformation properties.

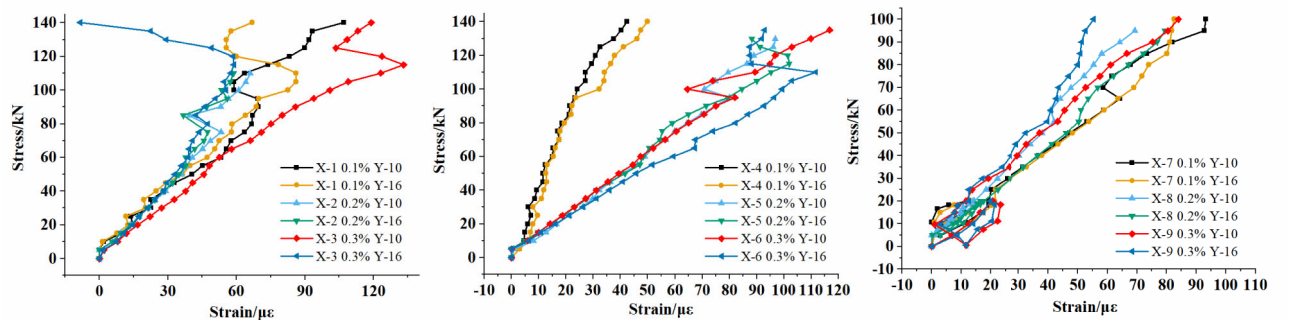

a specimens with reinforcement F1 **b** specimens with reinforcement F2 **c** specimens with reinforcement F3

Fig. 6 Load–strain curves of specimens with different basalt volume content

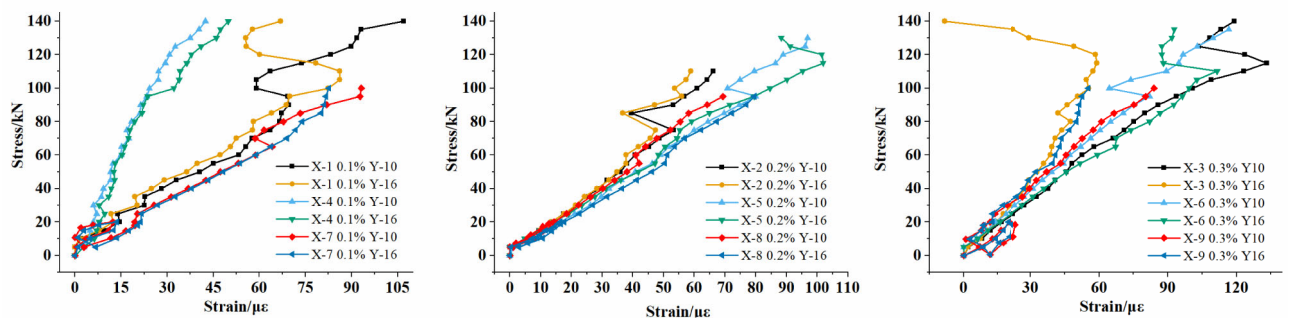

a specimens with 0.1% basalt fiber **b** specimens with 0.2% basalt fiber **c** specimens with 0.3% basalt fiber

Fig. 7 Load–strain curves under different reinforcement methods

Among all specimens, the standard track slab X0 was able to bear the largest load. When the load was less than 85 kN, the load–deflection curve of the standard track slab X0 was basically a straight line, and the track slab was in the elastic stage, while the elastic limit of specimens X1 and X2 was 50.06 kN and X3 was 55.02 kN. After that, with the increase in the load, the mid-span deflection increased significantly, and the track slab gradually exhibited nonlinear properties, indicating that the stiffness of the track slab gradually decreased. When the load reached 200 kN, the load and the mid-span deflection decreased rapidly, and the track slab almost failed. The total deflection of X0 reached a maximum value of 35.7 mm. Meanwhile, the failure loads of X1, X2, and X3 were 145 kN, 110 kN, and 180 kN with maximum deflections of 25.45 mm, 12.76 mm, and 31.05 mm, respectively.

When the loading load was less than 55 kN, all specimens exhibited almost the same linear portion, which ended at around 55 kN with a deflection of 5 mm. Since the reinforcement ratios of X1–X9 were smaller than that of X0, the same linear portion indicated that basalt fiber was beneficial for improving the elastic stiffness of the track slab, but there was no significant difference between the different basalt fiber content ranging from 0.1 to 0.3%. After the elastic limit, the load applied on the track slab was gradually carried by the steel skeleton, so that its failure load decreased with the reduction in the reinforcement ratio. Compared with specimens with reinforcement F2, specimens with reinforcement F1 showed a significant increase in the mid-span deflection of greater than 10%. At the same time, because of the reduction in reinforcement diameter, the stiffness degradation of the track slab with reinforcement F3 was more severe, and the flexural and compressive properties of the track slab were significantly reduced. Thus it can be seen that the reinforcement skeleton plays an important role in the stiffness of the track slab.

With different reinforcement arrangements, differences were observed in the influence of basalt fiber content on the failure load. For the reinforcement arrangement F1, the failure load of the specimen with 0.3% basalt fiber was the largest at 165 kN, while for the reinforcement arrangement F2, the failure load of the specimen with 0.1% basalt fiber was the largest at 150 kN. Because of the low reinforcement ratio, the failure loads of specimens with reinforcement arrangement F3 were much smaller than those of specimens with reinforcement arrangements F1 and F2, only about 90 kN, and the basalt fiber had almost no effect on the failure load.

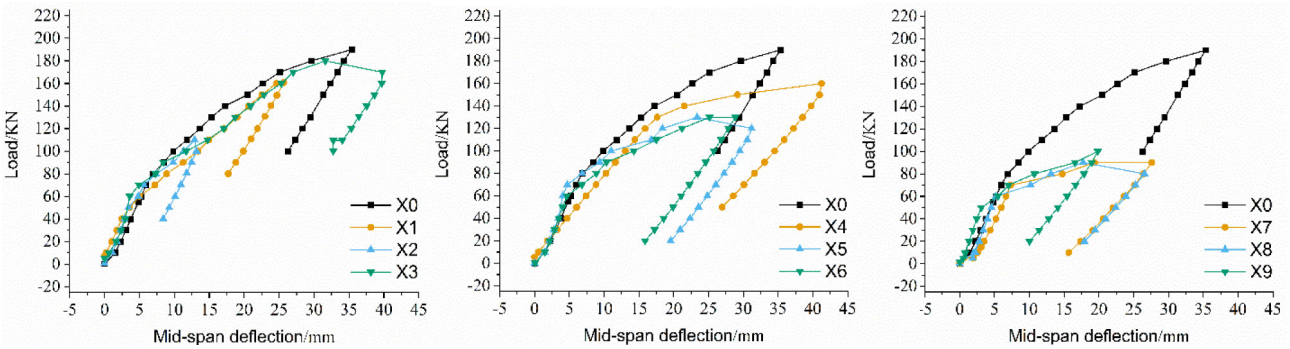

a specimens with reinforcement F1 **b** specimens with reinforcement F2 **c** specimens with reinforcement F3

Fig. 8 Load versus mid-span deflection for track slabs

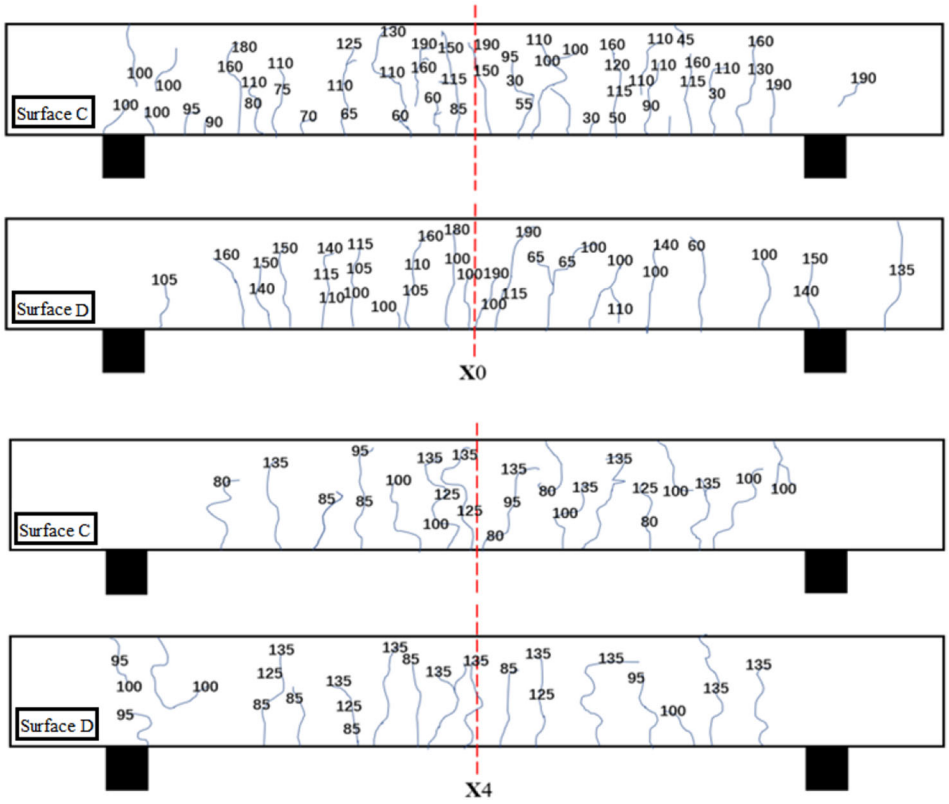

Fig. 9 Side cracks of track slabs X0 and X4

3.3 Cracks of the Track Slab

Before the static loading test, the initial cracks, including surface shrinkage cracks and surface damage cracks, were inspected with a 10-fold magnifying glass. All initial cracks were less than 0.04 mm in width. Except for the initial cracks, there were no obvious transverse or longitudinal cracks on the bottom and sides of the track slabs X0–X6 until the load reached 25 kN. The maximum crack widths of the standard track slab X0 and specimens X1–X6 were both less than 0.2 mm until the test load reached 1.5 times the elastic limit load, while the maximum crack widths of specimens X7–X9 exceeded 0.2 mm when the load was about 70 kN. For specimen X0, the initial maximum crack was 0.032 mm in width, and micro-cracks can be seen at the bottom when the load reached 25 kN. With the load increased to 35 kN, two initial cracks in the mid-span bottom rapidly propagated in the transverse direction. For specimen X4, the maximum initial crack was 0.02 mm in width, and new cracks were found at the bottom when the load reached 45 kN. When the load increased to 60 kN, the initial crack in the middle span of the bottom propagated as a longitudinal through-all crack. Cracks in both track slabs were mainly concentrated in the mid-span of the bottom and sides, which was near the load point, and the occurrence of side cracks lagged behind that of bottom cracks. It can be seen from Fig. 9 that new cracks and propagating cracks appeared on the sides of specimens X0 and X4 when the load reached 60 kN and 80 kN, respectively. Among all specimens, the total number of cracks and the number of through-all cracks of track slab X4 were the lowest. Thus, it can be concluded that track slab X4 had the best crack resistance.

4 Conclusion

Compared with the traditional cast-in-situ track slabs, the prefabricated new type of track slab is more suitable for the rapid development subway. Therefore, in this paper, we investigated the bearing performance of the new subway track slab with static load tests, and evaluated the influence of the reinforcement arrangements and the basalt fiber content on the bending performance and crack resistance. The results showed the following:

1. The elastic limit of the standard track slab specimen was the largest among all specimens, at 110 kN, and the increasing rate of the load–strain curve and the strain variable of the track slab were larger than that of the specimen with basalt fiber.
2. With an increase in the basalt fiber content in the range of 0.1–0.3%, the load–strain curve growth rate increased, and the stiffness and flexural resistance

decreased, indicating that the flexural performance of the new subway slab track declined with the increase in the basalt fiber volume content.

3. All the specimens exhibited a linear portion (elastic) and then a nonlinear portion (plastic) followed by flexural failure. When the loading load was less than 55 kN, all specimens exhibited almost the same linear portion, indicating that the addition of basalt fiber helps to improve the rigidity of the track slab in the elastic stage. During the plastic stage, the influence of the basalt fiber content on the failure load varied with different reinforcement arrangements. For the reinforcement arrangement F1, the failure load of the specimen with 0.3% basalt fiber was the largest at 165 kN, while for the reinforcement arrangement F2, the failure load of the specimen with 0.1% basalt fiber was the largest at 150 kN.
4. With the reinforcement arrangement F2 and 0.1% basalt fiber content, the specimen had the smallest load–strain curve growth rate and the best overall flexural performance and crack resistance. Specifically, its strain was 23.35 με at an elastic limit of 95 kN. The results showed that the structural flexural performance of the track slab could be improved by appropriately reducing the reinforcement amount and the diameter of the reinforcement and adding volume content of 0.1% basalt fiber. Based on the static bending tests, we found that the prefabricated new type track slab with the reinforcement arrangement F2 and a 0.1% basalt fiber content had the best flexural performance. The results will be useful for the design of the prefabricated slab ballastless track. But since all the track slabs are subjected to dynamic vehicle loads, the dynamic tests need to be researched further.

Acknowledgments This work was supported by the National Key Research and Development Program of China (Nos. 2021YFB2601000, 2021YFF0502100), the National Natural Science Foundation of China (Nos. 52208415), the Natural Science Foundation of Shaanxi Province of China (Nos. 2021JQ-255, 2022JQ-303, 2020JM-230), and China Postdoctoral Science Foundation (No. 2016M601312).

Availability of Data and Materials Not applicable.

Declarations

Conflict of interest The authors declare that they have no conflict of interest.

References

1. Yu C (2008) The solid track bed defect of urban mass transit and treatment. J Railw Eng Soc 12:83–86
2. Zhao Z, Qiao X (2014) Mechanism and prevention of the monolithic track bed disease damage in metro tunnels. Urban Mass Transit 17(12):98–100+117
3. Feng Q, Sun K, Chen H, Lei X (2021) Long-term prediction of fatigue crack growth in ballastless track of high-speed railway due to cyclic train load. Constr Build Mater 292:123375. https://doi.org/10.1016/j.conbuildmat.2021.123375
4. Zhao C, Wang P, Xi S, Duo M (2017) Theoretical simulation and experimental investigation of a rail damper to minimize short-pitch rail corrugation. Math Probl Eng 1:114. https://doi.org/10.1155/2017/2359404
5. Zhou S, Ji C (2014) Tunnel segment uplift model of earth pressure balance shield in soft soils during subway tunnel construction. Int J Rail Transp 4:221–238
6. Ma M, Li M, Wu Z, Wang W, Liu W (2019) Comparative experimental study on vibration reduction effect of floating slab track under metro train and fixed point hammering loads. China Railway Sci 40(05):28–34. https://doi.org/10.3969/j.issn.1001-4632.2019.05.05
7. Cao D (2018) Application of slab tracks to subways. Urban Rapid Rail Transit 31(01):109–114
8. Zhu ZT, Liu B, Zeng ZP, et al (2015) Study on the basic mechanical characteristics of CRTS Ill Slab Ballastless Track. In: International conference on mechatronics, electronic industrial and control engineering. Atlantis Press, Paris, pp 1475–1478
9. Ando K, Sunaga M, Aoki H, Haga O (2001) Development of slab track for Hokuriku Shinkansen line. Q Rep RTRI 42(1):35–41. https://doi.org/10.2219/rtriqr.42.35
10. Deng S-J, Zhang Y, Ren J-J, Yang K-X, Liu K, Liu M-M (2021) Evaluation index of CRTS III prefabricated slab track cracking condition based on interval AHP. Int J Struct Stab Dyn 21(14):2140013. https://doi.org/10.1142/S0219455421400137
11. Ye W, Deng S, Ren J, Xu X, Zhao K, Du W (2022) Deep learning-based fast detection of apparent concrete crack in slab tracks with dilated convolution. Constr Build Mater 329:127157. https://doi.org/10.1016/j.conbuildmat.2022.127157
12. Poveda E, Yu RC, Lancha JC, Ruiz G (2015) A numerical study on the fatigue life design of concrete slabs for railway tracks. Eng Struct 100:455–467. https://doi.org/10.1016/j.engstruct.2015.06.037
13. Jeongwon P, Sangkeun A, Jaehyun K (2017) Direct determination of dynamic properties of railway tracks for flexural vibrations. Eur J Mech A/Solids 61:14–21. https://doi.org/10.1016/j.euromechsol.2016.08.010
14. Gautier P (2015) Slab track: review of existing systems and optimization potentials including very high speed. Constr Build Mater 92:9–15. https://doi.org/10.1016/j.conbuildmat.2015.03.102
15. Gharighoran A, Hamidi A, Rafizadeh A (2012) Investigation of the subway slab tracks under different loading conditions. Case study: Isfahan Subway. Gut 32(7):784–786

16. Liu W, Lliu H, Zhao L, Shi LZ (2019) Design research on new slab-type track used in metro project. Railw Eng 59(01):76–80
17. He X, Cai X, Liang Y, Yao Z, Wang Q (2019) Dynamic tests and vibration reduction characteristics of vibration damping slab track in subway. Railw Stand Des 63(07):13–18
18. Liu Y, Xu Q (2020) Study on spatial mechanical properties of pre-cast slab track system in subway line. J Railw Sci Eng 17(07):1662–1670. https://doi.org/10.19713/j.cnki.43-1423/u.T20190842
19. Zeng J (2011) Study on the modification effect of basalt fiber on concrete. J China Foreign Highw 31(05):243–246